Mon. Not. R. Astron. Soc. **374,** 455–465 (2007) doi:10.1111/j.1365-2966.2006.11123.x

Local dark matter clumps and the positron excess

Daniel Cumberbatch★ and Joseph Silk★
Department of Astrophysics, University of Oxford, Keble Road, Oxford OX1 3RH

Accepted 2006 September 26. Received 2006 September 26; in original form 2006 February 28

ABSTRACT

It has been proposed that the excess in cosmic ray positrons at approximately 8 GeV, observed on both flights of the *High-Energy Antimatter Telescope* (*HEAT*) balloon experiment, may be associated with the annihilation of dark matter within the Milky Way halo. In this paper, we demonstrate how the self-annihilation of neutralino dark matter within local substructure can account for this excess, and we estimate the annihilation cross-section for several benchmark minimal supersymmetric (MSSM) models. We also demonstrate the changes in the permitted parameter space as the effects of tidal disruption become increasingly severe.

Key words: cosmic rays – dark matter.

1 INTRODUCTION

A large body of evidence pertaining to the existence of nonbaryonic cold dark matter (CDM) has been established over the past several decades, including the large-scale distribution of galaxies (see e.g. http://www.sdss.org), the study of primordial light-element abundances (Cyburt 2004), supernova data (Perlmutter et al. 1999) and the power spectrum of anisotropies observed in the cosmic microwave background (CMB) (Spergel et al. 2006). At the 2σ confidence level, the CDM energy density parameter is now $\Omega_{\rm CDM}\,h^2 = 0.111 \pm 0.004$.

A popular candidate for CDM is the lightest supersymmetric (SUSY) neutralino χ_1^0, which is a superposition of Binos, Winos and Higgsinos, which are the superpartners of the weak gauge and Higgs bosons. Consequently, the neutralino is electrically neutral and colourless, only interacting weakly and gravitationally and therefore very elusive to direct detection experiments. In many R-parity conserving SUSY models, the lightest neutralino, being the lightest SUSY particle (LSP), is stable (Weinberg et al. 1982). Consequently, within scenarios where present-day CDM exists as a result of thermal-freeze out, the dominant species of CDM is likely to include the LSP. The relic density of the LSP will then heavily depend on its mass and annihilation cross-section. Neutralinos [and weakly interacting massive particles (WIMPs) in general] are popular candidates for CDM because the expected values of these parameters are such that their corresponding relic densities are of the same order as the currently accepted value of $\Omega_{\rm CDM}$.

In 1994 and 1995, the *High-Energy Antimatter Telescope* (*HEAT*) observed a flux in cosmic ray positrons, very much in excess of theoretical predictions, and peaking close to 8 GeV (Coutu et al. 1999). This observation was confirmed by a subsequent flight in 2000 (Coutu et al. 2001). The effect was originally predicted in 1984 (Silk & Srednicki 1984), for both cosmic ray positrons and antiprotons. While the cosmic ray antiproton feature remains elusive, at least for theorists it is now a well-established idea that local dark matter annihilations are a possible source of the positrons contributing to the observed excess. Improved data are urgently required to validate the significance of this observation, and this is expected to be gathered in the near future by experiments like *PAMELA*, *AMS-02* and *Bess Polar*. In this paper, we summarize why extant models for local dark matter annihilations fail to adequately account for the current spectral data on the positron feature, and present a new model.

Studies in which the local (within several kpc) distribution of dark matter is considered to be smooth have concluded that the dark matter annihilation rate is insufficient to reproduce the observed positron flux (Baltz et al. 2001). This naturally leads to the idea of a non-uniform, or 'clumpy' dark matter distribution providing the overdensities necessary to elevate dark matter annihilation rates sufficiently to produce the observed excess. The distribution of such substructure can then be estimated through the use of simulations. Unfortunately, while simulations generally agree on the distribution of dark matter clumps, there is a (decreasing) divergence of opinion on the survival of the lightest clumps after the effects of hierachical structure formation and tidal stripping are considered (Diemand, Moore & Stadel 2005; Zhao et al. 2005; Angus & Zhao 2006; Goerdt et al. 2006).

We note that throughout this paper we will consider the LSP to be the lightest neutralino and proceed in using these two terms synonymously.

★E-mail: dtc@astro.ox.ac.uk (DC); silk@astro.ox.ac.uk (JS)

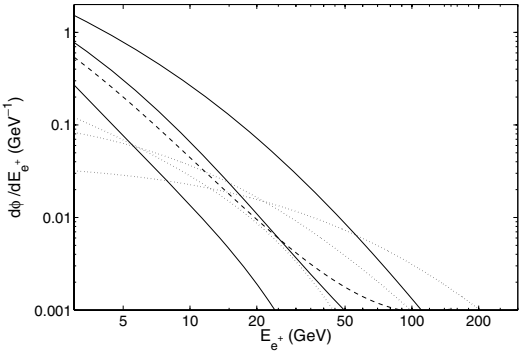

Figure 1. The positron energy spectra from neutralino annihilations for modes utilized in this paper. The solid lines represent the positron spectra, per annihilation, for $\chi_1^0\chi_1^0 \rightarrow b\bar{b}$, for neutralinos with masses of 50, 150 and 600 GeV. The dotted lines are the same, but correspond to the process $\chi_1^0\chi_1^0 \rightarrow \tau^+\tau^-$. The dashed lines correspond to the positron spectra from the process $\chi_1^0\chi_1^0 \rightarrow W^+W^-$, for a 150-GeV neutralino, where the spectrum from the process $\chi_1^0\chi_1^0 \rightarrow Z^0Z^0$ is very similar.

2 POSITRON SPECTRA FROM NEUTRALINO ANNIHILATION

Positrons can be produced in several neutralino annihilation modes. For example, positrons can result from the decay of gauge bosons produced in the processes $\chi_1^0\chi_1^0 \rightarrow Z^0Z^0$ or $\chi_1^0\chi_1^0 \rightarrow W^+W^-$, producing positrons of energy $\sim m_{\chi_1^0}/2$, where $m_{\chi_1^0}$ is the neutralino mass. A small amount of positrons result from the direct channel, $\chi_1^0\chi_1^0 \rightarrow e^+e^-$; however, such contributions are seldom significant to the overall positron flux. In addition, a continuum of positrons, extending to much lower energies, is produced from the cascades of particles emerging from annihilations. The spectrum of positrons produced in neutralino annihilations can vary significantly depending on the mass and annihilation modes of the LSP.

If the neutralino is lighter than the $W^{\pm}$ and Z^0 bosons, annihilations will be dominated by the process $\chi_1^0\chi_1^0 \rightarrow b\bar{b}$ with contributions by the process $\chi_1^0\chi_1^0 \rightarrow \tau^+\tau^-$ becoming significant for energies greater than $m_{\chi_1^0}/2$. For heavier LSPs, the annihilation products become more complex, often determined by several dominant annihilation modes including $\chi_1^0\chi_1^0 \rightarrow W^+W^-$, $\chi_1^0\chi_1^0 \rightarrow Z^0Z^0$ or $\chi_1^0\chi_1^0 \rightarrow t\bar{t}$ as well as $\chi_1^0\chi_1^0 \rightarrow b\bar{b}$ and $\chi_1^0\chi_1^0 \rightarrow \tau^+\tau^-$, depending on the gaugino/Higgsino fraction of the neutralino. In our calculations, the positron spectrum per annihilation per energy interval, $\mathrm{d}\phi/\mathrm{d}E_{\mathrm{e}^+}$, uses results from PYTHIA (Sjostrand et al. 2001), as is implemented in the DARKSUSY package (Gondolo et al. 2000).

In Fig. 1, we display results for positron spectra from neutralino annihilations for most important annihilation modes, as produced by Hooper, Taylor & Silk (2004). The solid lines represent the positron spectrum, per annihilation, for $\chi_1^0\chi_1^0 \rightarrow b\bar{b}$, for LSPs with masses of 50, 150 and 600 GeV. The dotted lines are the same, but from the process $\chi_1^0\chi_1^0 \rightarrow \tau^+\tau^-$. Bino-like annihilations typically produce a spectrum which is dominated by $b\bar{b}$ at low energies, with contributions from $\tau^+\tau^-$ only becoming important at energies above about half the LSP mass. For neutralinos with a dominant wino/higgsino component, annihilations to gauge bosons often dominate, with significant contributions above $m_{\mathrm{W}^{\pm}}$, where the process $\chi_1^0\chi_1^0 \rightarrow W^+W^- \rightarrow e^+e^-\nu\bar{\nu}$ is possible. The dashed lines represent positron spectra resulting from the process $\chi_1^0\chi_1^0 \rightarrow W^+W^-$ for a 150-GeV neutralino, where the spectrum corresponding to the process $\chi_1^0\chi_1^0 \rightarrow Z^0Z^0$ is very similar.

3 POSITRON PROPAGATION MODEL

Cosmic ray positrons diffuse through the interstellar medium (ISM) under the electromagnetic influence of the galactic magnetic field and background radiation. The spatial distribution of the galactic magnetic field is extremely complex, resulting in positron trajectories which are well approximated by random walks. Whilst traversing the ISM, the positrons radiate through synchrotron losses, owing to the surrounding magnetic fields, and by inverse-Compton scattering off both starlight and CMB background radiation (Webber, Lee & Gupta 1992).

Using $\epsilon = E_{\mathrm{e}^+}/1\,\mathrm{GeV}$, the diffusion-loss equation, for positrons of energy E_{e^+}, describing the above process is given by

$$\frac{\partial}{\partial t}\frac{\partial n_{e^+}}{\partial \epsilon} = \nabla \cdot \left[K(\epsilon, \boldsymbol{r})\nabla \frac{\partial n_{e^+}}{\partial \epsilon}\right] + \frac{\partial}{\partial \epsilon}\left[b(\epsilon, \boldsymbol{r})\frac{\partial n_{e^+}}{\partial \epsilon}\right] + Q(\epsilon, \boldsymbol{r}), \quad (1)$$

where $\partial n_{\mathrm{e}^+}/\partial\epsilon$ is the number density of positrons per unit energy interval, $K(\epsilon, \boldsymbol{r})$ is a diffusion coefficient, $b(\epsilon, \boldsymbol{r})$ is the rate of energy loss and $Q(\epsilon, \boldsymbol{r})$ is the source term.

We parametrize the diffusion coefficient and the rate of energy loss as follows:

$$K(\epsilon) = K_0\,(3^{\alpha} + \epsilon^{\alpha}) \approx 3 \times 10^{27}(3^{0.6} + \epsilon^{0.6})\ \mathrm{cm^2\ s^{-1}} \quad (2)$$

and

$$b(\epsilon) = \tau_E\,\epsilon^2 \approx 10^{-16}\,\epsilon^2\ \mathrm{s^{-1}}, \quad (3)$$

based on measurements of the nuclear composition cosmic rays (primarily by fitting to observations of the boron-to-carbon ratio) (Maurin et al. 2002), where in equations (2) and (3) we have assumed a spatially uniform galactic magnetic field. We then define K and b to be constant within a 'diffusion zone', which here is considered to be a radially-infinite cylindrical slab of thickness $2L \approx 4$ kpc, which is the maximum width consistent with observations (Webber et al. 1992; Maurin et al. 2002).

We solve equation (1) for the local positron flux, using the procedure described in Appendix A.

4 POSITRON AND ELECTRON BACKGROUNDS

In order to directly compare our results to the observations made by the *HEAT*, we must calculate the ratio of the local positron flux to the combined local positron and electron fluxes, called the 'positron fraction'. In order to do this, we require the local background spectra for secondary positrons, primary electrons and secondary electrons, and we propose that the primary positron component originates from neutralino annihilations. In the following, we make use of the parametrized fits to these spectra, calculated by Baltz & Edsjö (1999), and stated here (in units of $\mathrm{GeV}^{-1}\,\mathrm{cm}^{-2}\,\mathrm{s}^{-1}\,\mathrm{sr}^{-1}$), as follows:

$$\left(\frac{\mathrm{d}\Phi}{\mathrm{d}E_{e^+}}\right)_{\mathrm{prim}.e^-} = \frac{0.16\epsilon^{-1.1}}{1 + 11\epsilon^{0.9} + 3.2\epsilon^{2.15}}, \tag{4}$$

$$\left(\frac{\mathrm{d}\Phi}{\mathrm{d}E_{e^+}}\right)_{\mathrm{sec}.e^-} = \frac{0.70\epsilon^{0.7}}{1 + 110\epsilon^{1.5} + 600\epsilon^{2.9} + 580\epsilon^{4.2}}, \tag{5}$$

$$\left(\frac{\mathrm{d}\Phi}{\mathrm{d}E_{e^+}}\right)_{\mathrm{sec}.e^+} = \frac{4.5\epsilon^{0.7}}{1 + 650\epsilon^{2.3} + 1500\epsilon^{4.2}}. \tag{6}$$

These equations agree with their respective observational results to within 10–15 per cent for the relevent energy intervals. [For a more detailed account of the accuracy of these equations, refer to Strong & Moskalenko (2001).] The positron fraction is then calculated using

$$\frac{(\mathrm{d}\Phi/\mathrm{d}E)_{\mathrm{prim}.\,e^+} + (\mathrm{d}\Phi/\mathrm{d}E)_{\mathrm{sec}.\,e^+}}{(\mathrm{d}\Phi/\mathrm{d}E)_{\mathrm{prim}.\,e^-} + (\mathrm{d}\Phi/\mathrm{d}E)_{\mathrm{sec}.\,e^-} + (\mathrm{d}\Phi/\mathrm{d}E)_{\mathrm{prim}.\,e^+} + (\mathrm{d}\Phi/\mathrm{d}E)_{\mathrm{sec}.\,e^+}}. \tag{7}$$

5 DARK MATTER SUBSTRUCTURE

The standard cosmological model assumes that all structures in the universe originated from small-amplitude quantum fluctuations during an epoch of inflationary expansion shortly after the big bang. The linear growth of the resulting density fluctuations is then completely determined by their initial power spectrum $P(k) = k^n$, where for $n \geqslant 1$, clumps are formed with a wide range of scales proportional to k^{-1}. Subsequently, smaller clumps coalesce to form larger ones in a process of 'bottom–up' hierarchical structure formation, in which the mass distribution at any given redshift can be approximately determined through the use of numerical simulations.

Here, we utilize results from the unprecedentedly high-resolution simulations conducted by Diemand et al., aimed primarily at determining the properties of the smallest clumps to have formed in the galactic halo. The mass distribution of the clumps resulting from these simulations, which were terminated at $z = 26$, was found to be of the form $\mathrm{d}n_D/\mathrm{d}\log(M/\mathrm{M}_\odot) \propto (M/\mathrm{M}_\odot)^{-1}\exp[-(M/M_{\mathrm{cut-off}})^{-2/3}]$, with a lower mass cut-off $M_{\mathrm{cut-off}} \approx 8 \times 10^{-6}\,\mathrm{M}_\odot$. It was also recognized that for clump masses $M \gg M_{\mathrm{cut-off}}$, this distribution is very similar to that of a galactic halo at $z = 0$, which approximately scales as $\mathrm{d}n/\mathrm{dlog}\,M \propto M^{-0.9}$ (Diemand, Moore & Stadel 2004).

Therefore, we adopt the distribution $\mathrm{d}n_D/\mathrm{d}\log(M/\mathrm{M}_\odot)$ to describe the galactic subhalo population at the current epoch. We normalize this distribution so that the number density of clumps of masses between 10^{-6} and $10^{-5}\,\mathrm{M}_\odot$ is $500\,\mathrm{pc}^{-3}$ in the solar neighbourhood, deduced using the extrapolation procedure described in Diemand et al. (2005). [Unfortunately, a halo-to-halo scatter of approximately 4 is associated with this distribution, which we disregard in our calculations (Diemand, private communication).] We also invoke an upper mass cut-off, $M_{\mathrm{max}} \sim 10^{10}\,\mathrm{M}_\odot$, defined so that clumps of mass $M > M_{\mathrm{max}}$ possess an abundance of less than unity within the region contributing to the local positron flux.

We should highlight that here we are acknowledging clumpiness in the halo through a spatially *continuous* elevation in the density of dark matter, rather than the more realistic *discrete* distribution of clumps. Unsurprisingly, the former approach reproduces the *average* results obtained when considering the essentially infinite set of possible configurations of discrete clumps within the halo. This was demonstrated in the work by Lavalle et al. (2006), who deduced that the associated relative variance in the observed positron flux, as a result of the different clump configurations, is proportional to $M_{\mathrm{c}}^{1/2}$, where M_{c} is the typical clump mass, and diverges as $E_{\mathrm{e}^+} \rightarrow \mathrm{m}_\chi$. It is found that for $M_{\mathrm{c}} = 10^6\,\mathrm{M}_\odot$ and a universal clump boost factor, $B_{\mathrm{c}} \sim 100$, this relative variance is less than 5 per cent for $E_{\mathrm{e}^+} \leqslant 20$ GeV, which is where the positron excess observed by the *HEAT* is located. Since the clump mass distribution deduced by Diemand et al. indicates that $M_{\mathrm{c}} \sim 10^{-6}\,\mathrm{M}_\odot$, it seems very unlikely that such a variance will significantly affect our conclusions, and we use this to strengthen our use of a spatially continuous elevation in dark matter density as a way of acknowledging clumpiness in the galactic halo.

The rate of dark matter annihilations within a clump crucially depends on its density profile. Here, we adopt the widely used profile proposed by Navarro, Frenk & White (1997, hereafter NFW):

$$\rho(r) = \frac{\rho_0}{(r/r_{\mathrm{s}})[1 + (r/r_{\mathrm{s}})]^2}, \tag{8}$$

which provides a good fit to the lightest clumps produced in Diemand et al.'s simulations. The scalelength r_s is given by

$$r_s = \frac{c_{vir}}{r_{vir}}, \tag{9}$$

where r_{vir} is the virial radius and c_{vir} is the virial concentration, which at $z = 26$ was found to lie in the range $1.6 < c_{vir} < 3$ for the clumps in Diemand et al.'s simulations. However, it proved more convenient to use the equivalent relation

$$r_s = \frac{c_{nfw}}{r_{200}}, \tag{10}$$

where r_{200} is the radius at which the density is equal to 200 times the cosmological critical density ρ_c, and c_{nfw} is a concentration parameter which can be easily related to c_{vir} (see Appendix B).

According to Bullock et al. (2001), $r_s(z) \sim$ constant for a given clump mass, for any given redshift (although r_{vir} and c_{vir} both increase with time). Therefore, we adopt a universal clump density profile of the form

$$\rho = \frac{\rho_0}{\left[(c_{nfw}/r_{200})_{z=26}\, r\right]\left\{1 + \left[(c_{nfw}/r_{200})_{z=26}\, r\right]\right\}^2}, \tag{11}$$

for $0 < r < r_{200}(z)$, where we note that r_{200} is a function of the clump mass, and ρ_0 is a normalization constant chosen so that $\rho((r_{200})_{z=26}) = 200(\rho_c)_{z=26}$.

Since it was observed by Diemand et al. that there was no strong correlation between clump mass and concentration, we compare results when adopting a universal value of $(c_{vir})_{z=26} = 1.6$ and 3, which correspond to $(c_{nfw})_{z=26}$ values of 1.02 and 1.82, respectively (obtained using expression 40 of Appendix B, with $\Delta_{vir} = 200$, which is the same value as that used by Diemand et al.).

It is also important to consider the loss of mass by clumps resulting from tidal stripping by stars as the clumps traverse the galactic halo. In this study, we consider a scenario where the surviving mass fraction of a clump f, after a given duration Δt, is a constant, independent of the clump mass, and we compare results using several different values of f.

The notion of a universal tidal stripping parameter is consistent with the calculation by Zhao et al. (2005), who demonstrated that

$$\ln \frac{1}{f} \propto \frac{\langle \rho_* \rangle}{\rho_{core}^{1/2}} \Delta t, \tag{12}$$

where $\langle \rho_* \rangle$ is the average stellar densiity along the clump orbit, ρ_{core} is an effective 'core' density of the clump and Δt is the time period considered. Since the majority of clumps have similar orbital parameters (Zhao et al. 2005), and since we have adopted a universal density profile (11), equation (12) implies that f is independent of the clump mass.

6 POSITRON SPECTRA FROM DARK MATTER SUBSTRUCTURE

We consider the following four different neutralino models.

First, a 50-GeV neutralino with an annihilation branching ratio of 0.96 to $b\bar{b}$ and 0.04 to $\tau^+\tau^-$. Such a particle could be gaugino-like or Higgsino-like, since for masses below the gauge boson masses, these modes dominate for either case (designated as model 1).

Secondly, we consider two examples of a 150-GeV neutralino. One which annihilates as described in model 1 (designated as model 2), and another which annihilates entirely to W^+W^- or Z^0Z^0 (designated as model 4). Such neutralinos are typically gaugino-like and Higgsino-like, respectively.

Finally, we consider 600-GeV neutralinos, which annihilate to $b\bar{b}$ with a ratio of 0.87 and to $\tau^+\tau^-$ or t^+t^- in the remaining time (designated as model 3). (We note that even though we do not explicitly calculate results for a model involving 600-GeV Higgsino-dominated neutralinos, which primarily decay to gauge bosons and partially to Higgs bosons, the resulting positron spectra per annihilation are likely to be very similar to that of model 3.)

Although these models do not fully encompass the extensive parameter space currently available to neutralinos, they do represent effective minimal supersymmetric (MSSM) benchmarks. Furthermore, the results relevant to neutralinos which possess a mixture of the properties of the above models can be inferred from interpolating between our results.

Figs 2–5 display the positron fraction as a function of positron energy, calculated for each of the four MSSM models outlined above.

The thermally averaged product of the low-velocity annihilation cross-section and relative speed of dark matter particles, $\langle \sigma \upsilon \rangle$, was left as a free parameter and varied to fit our results to observations. In each figure, the solid line displays the positron fraction which fitted best to the 1σ error bars of the 94–95 (red) and 2000 (blue) *HEAT* data. The dashed lines correspond to positron fractions where χ^2, calculated for the 12 data points, differs by unity from the corresponding best-fitting value (1σ results). Finally, the dot–dashed lines correspond to the non-exotic background spectrum, discussed in Section 2. The results are summarized in Table 1.

7 ASSESSMENT

The results displayed in Figs 2–5 indicate that neutralino annihilations within local dark matter substructure can give rise to positron fractions which correspond well to observations, with χ^2 between 2.7 and 5.3, for values of $\langle \sigma \upsilon \rangle$ ranging from 3×10^{-28} cm^3 s^{-1} for 50-GeV neutralinos, to 4×10^{-26} cm^3 s^{-1} for 600-GeV neutralinos.

The majority of the determined values of $\langle \sigma \upsilon \rangle$ are one or two orders of magnitude smaller than the canonical estimate of 3×10^{-26} cm^3 s^{-1}, determined from relic density calulations (Bertone, Hooper & Silk 2005). However, many conventional MSSM models exist in which this

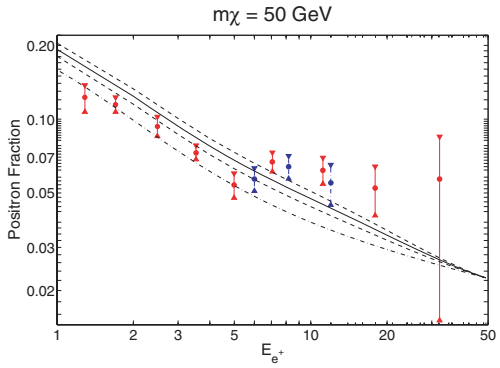

Figure 2. The calculated positron fraction as a function of positron energy (in GeV), for a 50-GeV neutralino which annihilates to $b\bar{b}$ 96 per cent of the time and 4 per cent to $\tau^+\tau^-$ (designated as model 1). The error bars displayed are for the 1994–95 (solid/red online) and 2000 (dashed/blue online) *HEAT* data. The solid line represents the spectra which best fit the data. The best-fitting χ^2 for this model is approximately 5.3 (for 12 data points). The dashed lines represent the spectra corresponding to the 1σ fits to the observations, where the normalization of the positron flux was considered to be a free parameter. The dot–dashed line represents the non-exotic background contribution to the positron fraction.

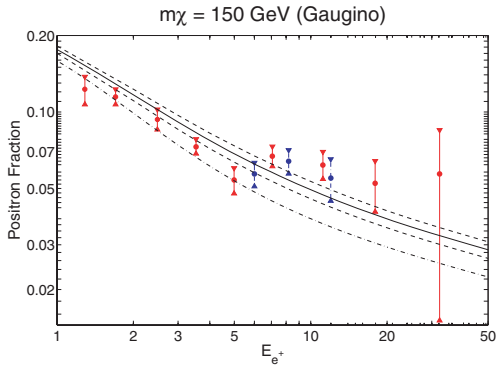

Figure 3. The calculated positron fraction as a function of positron energy (in GeV), for a 150-GeV neutralino which annihilates to $b\bar{b}$ 96 per cent of the time and 4 per cent to $\tau^+\tau^-$ (designated as model 2). The best-fitting χ^2 for this model is 4.4 (for 12 data points). Otherwise, the same as in Fig. 2.

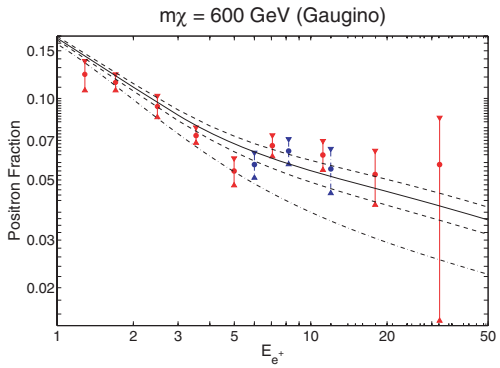

Figure 4. The calculated positron fraction as a function of positron energy (in GeV), for a 600-GeV neutralino which annihilates 87 per cent to $b\bar{b}$ and 13 per cent to $\tau^+\tau^-$ or t^+t^- (designated as model 3). The best-fitting χ^2 for this model is 2.7 (for 12 data points). Otherwise, the same as in Fig. 2.

approximation is grossly violated and are easily able to accommodate the majority of the results obtained, where the number of such models rapidly increases for lighter neutralinos, especially near 50 GeV (Hooper & Silk 2005).

As expected, we observe that the best-fitting values of $\langle\sigma\upsilon\rangle$ increase as the dark matter clumps become increasingly stripped, and decrease as we increase their concentration, where the latter makes sense since a larger concentration implies that an increasing proportion of the clump mass is contained within a smaller radius. However, we observe that even with up to 99 per cent stripping and varying the clump concentration over the entire range observed by Diemand et al., the best-fitting values of $\langle\sigma\upsilon\rangle$ do not change by more than a factor of 2.

We note that, of course, in reality the density of the clumps cannot diverge at their centres, as an NFW profile suggests, but are likely to possess uniformly dense cores containing of the order of 1 per cent of their total mass (Zhao et al. 2005). The stripping and eventual

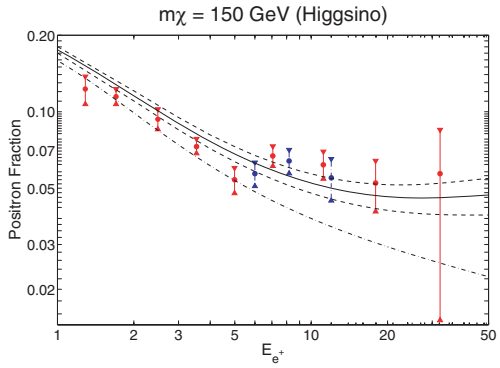

Figure 5. The calculated positron fraction as a function of positron energy (in GeV), for a 150-GeV neutralino which annihilates entirely to W^+W^- or Z^0Z^0 (designated as model 4). The best-fitting χ^2 for this model is 3.1 (for 12 data points). Otherwise, the same as in Fig. 2.

Table 1. Values of the product $\langle\sigma\upsilon\rangle$, in $\mathrm{cm}^3\,\mathrm{s}^{-1}$, which give rise to positron fractions which best fit the *HEAT* observations, for the four MSSM models considered, for $M_{\mathrm{cut-off}} = 8 \times 10^{-6}$ and various values of c and f. 1σ error ranges are also displayed.

f	$c_{\mathrm{vir}} = 3$ Best fit/10^{-28}	$1\sigma/10^{-28}$	$c_{\mathrm{vir}} = 1.6$ Best fit/10^{-28}	$1\sigma/10^{-28}$
Model 1				
1	2.6	1.6–3.6	8.0	5.0–10.9
0.1	2.8	1.8–3.8	8.6	5.4–11.8
0.01	4.8	3.0–6.5	15.0	9.5–20.5
Model 2				
1	4.9	3.1–6.6	14.8	9.6–19.9
0.1	5.2	3.4–7.1	16.0	10.4–21.5
0.01	8.9	5.8–12.0	28.2	18.4–37.9
Model 3				
1	20.5	13.4–27.1	61.9	42.3–81.5
0.1	21.2	14.9–28.9	66.9	45.7–88.0
0.01	37.0	25.3–48.7	118.6	81.1–156.1
Model 4				
1	6.1	4.1–8.2	18.7	12.2–25.1
0.1	6.6	4.4–8.7	20.2	13.6–26.8
0.01	11.1	7.5–14.7	35.3	23.9–46.7

disintegration of these cores is a topic of much debate and is currently being investigated (Green & Goodwin 2006). We therefore do not display results for $f < 0.01$, since it is unknown as to whether these cores can survive such severe levels of disruption.

However, in Table 2, we display results similar to those in Table 1, now for $M\mathrm{cutoff} = 10^6\,\mathrm{M}_\odot$, corresponding to the typical mass resolution of simulations of the galactic dark matter halo, in order to simulate the destruction of lighter clumps. We observe that the best-fit values of $\langle\sigma\upsilon\rangle$ are no more than five times their corresponding values in Table 1, but are more consistent with the canonical value and consequently consistent with a larger number of MSSM models.

We should also note that these results may be slightly modified when acknowledging flux contributions from tidal streams resulting from material stripped off clumps (Zhao et al. 2005). However, owing to the significantly lower densities of these streams, compared to the clumps from which they originate, it is very unlikely that such effects will significantly alter our results.

8 CONCLUSIONS

For each of the four benchmark supersymmetric models considered, we solved the diffusion-loss equation for the local positron flux resulting from neutralino annihilations within local dark matter substructure. We utilized results from the unprecedentedly high-resolution simulations, conducted by Diemand et al., to estimate the mass distribution of subhaloes at the current epoch and to justify the assignment of a universal NFW density profile to each clump. We investigated the changes in the flux when invoking different degrees of tidal mass loss suffered by each clump, to simulate the effects of stellar encounters.

Our results indicate that neutralino annihilations within local dark matter substructure can give rise to positron fractions which correspond well to the observations by the *HEAT*, for values of $\langle\sigma\upsilon\rangle$ ranging from 3×10^{-28} $\mathrm{cm}^3\,\mathrm{s}^{-1}$ for 50-GeV neutralinos to 4×10^{-26} $\mathrm{cm}^3\,\mathrm{s}^{-1}$ for

Table 2. Values of the product $\langle \sigma \upsilon \rangle$, in $\mathrm{cm}^3\ \mathrm{s}^{-1}$, which give rise to positron fractions which best fit the *HEAT* observations, for the four MSSM models considered, for $M_{\mathrm{cut-off}} = 10^6$ and various values of c and f. 1σ error ranges are also displayed.

f	$c_{\mathrm{vir}} = 3$ Best fit$/10^{-28}$	$1\sigma/10^{-28}$	$c_{\mathrm{vir}} = 1.6$ Best fit$/10^{-28}$	$1\sigma/10^{-28}$
Model 1				
1	10.2	6.4–13.9	30.8	19.5–42.1
0.1	10.8	6.8–14.8	33.3	21.1–45.5
0.01	18.5	11.7–25.3	59.0	37.3–80.7
Model 2				
1	18.4	11.9–24.8	55.4	36.0–74.9
0.1	19.6	12.7–26.5	60.0	39.1–81.0
0.01	33.2	21.7–44.8	105.6	68.5–142.8
Model 3				
1	76.1	51.2–100.8	231.2	157.2–305.3
0.1	81.3	55.0–107.5	250.5	170.0–331.0
0.01	139.1	947.1–183.6	442.6	300.6–584.5
Model 4				
1	23.0	15.5–30.5	69.5	46.7–92.3
0.1	24.6	16.6–32.5	75.3	50.8–99.9
0.01	41.7	28.0–55.3	132.6	89.0–176.2

600-GeV neutralinos. Despite the fact that the majority of the values of $\langle \sigma \upsilon \rangle$ determined were at least an order of magnitude smaller than the canonical value of $3 \times 10^{-26}\ \mathrm{cm}^3\ \mathrm{s}^{-1}$, approximated from relic density calulations, we highlight that many conventional MSSM models exist in which this approximation is grossly violated and are easily able to accomodate our results, where the number of such models rapidly increases for lighter neutralinos, especially near 50 GeV.

We observed that even with up to 99 per cent stripping, and varying the clump concentration over a range consistent with the results presented by Diemand et al., the best-fitting values of $\langle \sigma \upsilon \rangle$ do not change by more than a factor of 2. We also observed that even if we change the lower mass cut-off in our mass distribution from 8×10^{-6} to $10^6\ \mathrm{M}_\odot$, the best-fitting values of $\langle \sigma \upsilon \rangle$ increase by no more than a factor of 5, but are consequently more consistent with a larger region of MSSM parameter space.

ACKNOWLEDGMENT

We would like to thank S. Nussinov, D. Hooper and J. Diemand for various discussions with us on this topic.

REFERENCES

Angus G. W., Zhao H. S., 2006, preprint (astro-ph/0608580)
Baltz E. A., Edsjö J., 1999, Phys. Rev. D, 59, 023511
Baltz E. A., Edsjo J., Freese K., Gondolo P., 2001, Phys. Rev. D, 65, 063511
Bertone G., Hooper D., Silk J., 2005, Phys. Rep., 405, 5
Bullock J. S., Kolatt T. S., Sigad Y., Somerville R. S., Kravtsov A. V., Klypin A. A., Primack J. R., Dekel A., 2001, MNRAS, 321, 559
Coutu S. et al., 1999, Astropart. Phys., 11, 429
Coutu S. et al. HEAT-pbar Collaboration, 2001, Proc. 27th Internat. Cosmic Ray Conf., Positron measurements ith the HEAT-pbar instrument. Online reference: http://www.copernicus.org/icrc/papers/ici7190-p-pdf
Cyburt R. H., 2004, Phys. Rev. D, 70, 023505
Diemand J., Moore B., Stadel J., 2005, Nat, 433, 389
Diemand J., Moore B., Stadel J., 2004, MNRAS, 352, 535
Goerdt T., Gnedin O. Y., Moore B., Diemand J., Stadel J., 2006, preprint (astro-ph/0608495)
Gondolo P., Edsjo J., Bergstrom L., Ullio P., Baltz E., 2000, preprint (astro-ph/0012234)
Green A. M., Goodwin S. P., 2006, preprint (astro-ph/0604142)
Hooper D., Taylor J., Silk J., 2004, Phys. Rev. D, 69, 103509
Hooper D., Silk J., 2005, Phys. Rev. D, 71, 083503
Lavalle J., Pochon J., Salati P., Talliet R., 2006, preprint (astro-ph/0603796)
Maurin D., Donato F., Taillet R., Salati P., 2002, A&A, 394, 1039
Navarro J. F., Frenk C. S., White S. D. M., 2006, ApJ, 490, 493
Perlmutter S. et al. Supernova Cosmology Project Collaboration, 1999, ApJ, 517, 565
Spergel D. N. et al., 2006, preprint (astro-ph/0603449)
Silk J., Srednicki M., 1984, Phys. Rev. Lett., 53, 624
Sjostrand T., Eden P., Friberg C., Lonnblad L., Miu G., Mrenna S., Norrbin E., 2001, Comput. Phys. Commun., 135, 238

Strong A. W., Moskalenko I. V., 2001, Adv. Space Res., 27, 717
Webber W. R., Lee M. A., Gupta M., 1992, ApJ, 390, 96
Weinberg S., 1982, Phys. Rev. D, 26, 287
Zhao H., Taylor J. E., Silk J., Hooper D., 2005, preprint (astro-ph/0508215v1)

APPENDIX A: DERIVATION OF THE STEADY-STATE POSITRON FLUX

Here, we derive in detail the steady-state solution to the diffusion-loss equation (1), for positrons of energy E_{e^+}, given by

$$\frac{\partial}{\partial t}\frac{\partial n_{e^+}}{\partial E_{e^+}} = \nabla\cdot\left[K(E_{e^+},\boldsymbol{r})\nabla\frac{\partial n_{e^+}}{\partial E_{e^+}}\right] + \frac{\partial}{\partial E_{e^+}}\left[b(E_{e^+},\boldsymbol{r})\frac{\partial n_{e^+}}{\partial E_{e^+}}\right] + Q(E_{e^+},\boldsymbol{r}). \tag{A1}$$

Our treatment is very similar to that described in Edsjo et al. (1998), except that several unnecessary assumptions made in that derivation are omitted here, making our solution slightly more general.

We first re-express equation (A1) in terms of the dimensionless parameter $u = 1/\epsilon = 1\,\mathrm{GeV}/E_{e^+}$, and re-write the diffusion coefficient, given by (2), as $K = K_0 h(u)$, which gives

$$\frac{1}{h(u)}\frac{\partial}{\partial u}\frac{\partial n_{e^+}}{\partial u} = K_0\tau_E\nabla^2\frac{\partial n_{e^+}}{\partial u} - \tau_E[u^2h(u)]^{-1}Q(\epsilon(u),\boldsymbol{r}), \tag{A2}$$

where we have used equation (3) for the energy-loss rate, b. We now re-express equation (A2) in terms of the variable v, where $h(u) = \mathrm{d}v/\mathrm{d}u$. Provided that $h(u)$ is differentiable, we obtain

$$\frac{\partial}{\partial v}\frac{\partial n_{e^+}}{\partial u} = K_0\tau_E\nabla^2\frac{\partial n_{e^+}}{\partial u} - \tau_E[u^2h(u)]^{-1}Q(\epsilon(v),\boldsymbol{r}). \tag{A3}$$

Now making the substitutions

$$w(v) = -\frac{\mathrm{d}\epsilon}{\mathrm{d}v} = [u^2h(u)]^{-1}, \tag{A4}$$

and

$$F(v,\boldsymbol{r}) = \frac{\partial n_{e^+}(v,\boldsymbol{r})}{\partial u(v)}, \tag{A5}$$

equation (A3) becomes

$$\frac{\partial}{\partial v}F(v,\boldsymbol{r}) = K_0\tau_E\nabla^2F(v,\boldsymbol{r}) - \tau_E w(v)Q(\epsilon(v),\boldsymbol{r}). \tag{A6}$$

As stated in Edsjo et al. (1998), equation (A6) is analogous to an inhomogeneous heat equation. The spatial variables are exactly analogous, while v is analogous to time. Since $v = \int h(u)\,\mathrm{d}u = 3^\alpha u + (1-\alpha)^{-1}u^{1-\alpha}$, we find that v is a monotonically increasing function for $\alpha < 1$, and therefore is appropriately analogized to time.

Considering the above, we can write the solution of the steady-state positron number density as an integral over the effective source term $-\tau_E w(v)Q(\epsilon\,(v),\boldsymbol{r})$, of equation (A6), multiplied by a Green's function.

We first solve for the free Green's function G_{free}, which satisfies

$$\frac{\partial}{\partial v}G_{\mathrm{free}}(v-v',\boldsymbol{r}-\boldsymbol{r}') - K_0\tau_E\nabla^2G_{\mathrm{free}}(v-v',\boldsymbol{r}-\boldsymbol{r}') = \delta(v-v')\delta(\boldsymbol{r}-\boldsymbol{r}'), \tag{A7}$$

which is identical to equation (A6) with an effective source term $\delta(v-v')\delta(\boldsymbol{r}-\boldsymbol{r}')$, which is proportional to the source term for a monoenergetic point source with $v = v'$, located at $\boldsymbol{r} = \boldsymbol{r}'$. Taking the (spatial) Fourier transform of equation (A7), we obtain

$$\frac{\partial}{\partial v}\tilde{G}_{\mathrm{free}}(v-v',\boldsymbol{k}) + K_0\tau_Ek^2\tilde{G}_{\mathrm{free}}(v-v',\boldsymbol{k}) = (2\pi)^{-3/2}\delta(v-v')\exp(-\mathrm{i}\boldsymbol{k}\cdot\boldsymbol{r}'), \tag{A8}$$

where $\tilde{G}_{\mathrm{free}}$ is the Fourier transform of G_{free}. Multiplying each side of equation (A8) by the integrating factor $I = \exp(K_0\tau_Ek^2v)$ and integrating over v, we obtain

$$\tilde{G}(v-v',\boldsymbol{k}) = (2\pi)^{-3/2}\exp(-K_0\tau_Ek^2(v-v'))\times\exp(-\mathrm{i}\boldsymbol{k}\cdot\boldsymbol{r})\theta(v-v'), \tag{A9}$$

where we have invoked the condition $G_{\mathrm{free}} = 0$ (and therefore $\tilde{G}_{\mathrm{free}} = 0$) for $v = 0$ (i.e. at infinite energy). Finally, we take the inverse Fourier transform of equation (A9), to obtain

$$G_{\mathrm{free}}(v-v',\boldsymbol{r}-\boldsymbol{r}') = (2\pi)^{-3/2}\int_{\boldsymbol{k}}\tilde{G}(v-v',\boldsymbol{k})\exp(\mathrm{i}\boldsymbol{k}\cdot\boldsymbol{r})\mathrm{d}^3\boldsymbol{k}, \tag{A10}$$

which evaluates to

$$G_{\rm free}(v-v', \boldsymbol{r}-\boldsymbol{r}') = \left[\pi D(v, v')\right]^{-3} \exp\left(-\frac{(\boldsymbol{r}-\boldsymbol{r}')^2}{[D(v, v')]^2}\right), \tag{A11}$$

where $D(v, v') = [4K_0\tau_E(v-v')]^{1/2}$.

As described in Section 3, our chosen diffusion zone is an infinite cylindrical slab of thickness $2L$, where positrons located outside this region simply free-stream. Therefore, the steady-state positron distribution must therefore vanish at $r = \infty$ and $|z| > L$. Ignoring contributions from sources outside the diffusion zone, and then from the form of the diffusion equation, the positron distribution will be zero for $|z| > L$ if it is zero at $z = \pm L$. Therefore, in order to obtain our desired positron distribution within the diffusion zone, we can use a Green's function which simply vanishes at the boundaries of our diffusion zone. To do this, we adopt the solution proposed by Edsjo et al. (1998), which utilizes a set of image charges,

$$x'_n = x', \;\; y'_n = y', \;\; z'_n = 2Ln + (-1)^n z', \tag{A12}$$

to find the required Green's function,

$$G_{2L}(v-v', \boldsymbol{r}-\boldsymbol{r}') = \sum_{n=-\infty}^{\infty} (-1)^n G_{\rm free}(v-v', \boldsymbol{r}-\boldsymbol{r}'_n). \tag{A13}$$

As described above, the steady-state positron distribution can then be expressed as the following integral:

$$\begin{aligned}\frac{\partial n}{\partial \epsilon} &= \tau_E \epsilon^{-2} \int_0^{v(\epsilon)} {\rm d}v' w(v') \\ &\quad \times \int {\rm d}^3\boldsymbol{r}' G_{2L}\left(v(\epsilon) - v', \boldsymbol{r}-\boldsymbol{r}'\right) Q(\epsilon(v'), \boldsymbol{r}').\end{aligned} \tag{A14}$$

Using equation (A4), we can then conveniently re-express equation (A14) as

$$\begin{aligned}\frac{\partial n}{\partial \epsilon} &= \tau_E \epsilon^{-2} \int_\epsilon^{\infty} {\rm d}\epsilon' \\ &\quad \times \int {\rm d}^3\boldsymbol{r}' G_{2L}\left(v(\epsilon) - v'(\epsilon'), \boldsymbol{r}-\boldsymbol{r}'\right) Q(\epsilon, \boldsymbol{r}').\end{aligned} \tag{A15}$$

Now we must construct an appropriate source function, Q. To do this, we only consider contributions from dark matter substructure, ignoring the contribution from the smooth component of the halo, which we calculate to be approximately 10^{-4} times the substructure component. As described in Section 4, we assume each clump to have an NFW profile, $\rho_{\rm NFW}(c, r_{200}(M))$, with concentration, c, and maximum radius, $r_{200}(c, M)$, determined by c and the clump mass, M. The rate of production of positrons of energy ϵ GeV, is then

$$\frac{\langle\sigma v\rangle}{m_\chi^2}\frac{{\rm d}\phi}{{\rm d}\epsilon}\int_0^{r_{200}(c,M)} \rho^2(r') 4\pi r'^2 \, {\rm d}r' = \frac{\langle\sigma v\rangle}{m_\chi^2}\frac{{\rm d}\phi}{{\rm d}\epsilon} f^2_{\rm NFW}(c, M), \tag{A16}$$

where $\langle\sigma v\rangle$ is the thermally averaged, low-velocity annihilation cross-section multiplied by relative speed and ${\rm d}\phi/{\rm d}\epsilon$ is the number of positrons produced per annihilation per energy interval.

We must now multiply equation (A16) by the correctly normalized density of clumps. As described in Section 4, we utilize the clump distribution, ${\rm d}\,n_D(M)/{\rm d}\log M$, determined by Diemand et al., normalized to a local clump density of 500 pc^{-3}, and like Diemand et al., we assume that this normalization is proportional to the underlying halo density profile, $\rho_{\rm halo}$. For simplicity, we choose the halo profile to be a 'cylindrically' symmetric NFW profile:

$$\rho_{\rm halo}(r) = \frac{\rho_0}{(r/R)[1+(r/R)]^2}, \tag{A17}$$

where r is the cylindrical radial coordinate, $R \approx 20$ kpc and ρ_0 is a constant. The correctly normalized, spatially-dependent mass distribution of clumps is then

$$\begin{aligned}\frac{{\rm d}n(r, M)}{{\rm d}\log M} &= \frac{\rho_{\rm halo}(r)}{\rho_{\rm halo}(r = {\rm R}_\odot)}\frac{{\rm d}n_D(M)}{{\rm d}\log M} \\ &\simeq \frac{0.86}{(r/R)[1+(r/R)]^2}\frac{{\rm d}n_D(M)}{{\rm d}\log M},\end{aligned} \tag{A18}$$

where ${\rm R}_\odot \approx 8.5$ kpc, is the approximate distance between the Earth and the Galactic Centre.

Considering the above, the source function is given by

$$Q(\epsilon, r) = \frac{\langle\sigma v\rangle}{m_\chi^2}\frac{{\rm d}\phi}{{\rm d}\epsilon}\int_{M_{\rm min}}^{M_{\rm max}} f^2_{\rm NFW}(c, M)\frac{{\rm d}n(r, M)}{{\rm d}\log M}{\rm d}\log M, \tag{A19}$$

where $M_{\rm min} \sim 10^{-6}\,{\rm M}_\odot$ and $M_{\rm max} \sim 10^{10}\,{\rm M}_\odot$, as discussed in Section 4.

Substituting expressions (A13), (A18) and (A19) into equation (A15), evaluated at $z = 0$ and $r = \mathrm{R}_\odot$, we obtain the required (local) positron number density

$$\left(\frac{\partial n_{e^+}}{\partial \epsilon}\right) = \frac{\langle \sigma \upsilon \rangle \tau_E}{\pi^{3/2}(m_\chi \epsilon)^2} \int_{M_{\min}}^{M_{\max}} f^2_{\mathrm{NFW}}(c, M) \frac{\mathrm{d}n_D(M)}{\mathrm{d}\log M} \mathrm{d}\log M$$
$$\times \int_\epsilon^\infty \mathrm{d}\epsilon' \left\{ D[v(\epsilon), v'(\epsilon')] \right\}^{-3} \frac{\mathrm{d}\phi}{\mathrm{d}\epsilon'} \sum_{n=-\infty}^{\infty} (-1)^n$$
$$\times \int_{-L}^{L} \mathrm{d}z' \exp\left[-\left(\frac{(-1)^n z' + 2Ln}{D\,[v(\epsilon), v'(\epsilon')]} \right)^2 \right]$$
$$\times \int_0^\infty \mathrm{d}r' r' \frac{0.86}{(r'/R)(1 + (r'/R))^2}$$
$$\times \exp\left(-\frac{\mathrm{R}_\odot^2 + r'^2}{\{D\,[v(\epsilon), v'(\epsilon')]\}^2} \right)$$
$$\times \int_0^{2\pi} \mathrm{d}\theta' \exp\left(\frac{2 r r' \cos\theta'}{\{D\,[v(\epsilon), v'(\epsilon')]\}^2} \right). \tag{A20}$$

The θ' integral evaluates to $2\pi I_0$, where I_0 is a modified bessel function of the first kind and the z' integral evaluates to the following sum of error functions:

$$H(L, D) = \pi^{1/2} D \left(\mathrm{erf}\left(\frac{L}{D}\right) + \sum_{m=1}^{\infty} \left\{ \mathrm{erf}\left[\frac{(4m-3)L}{D}\right] \right.\right.$$
$$\left.\left. + \mathrm{erf}\left[\frac{(4m+1)L}{D}\right] - 2\mathrm{erf}\left[\frac{(4m-1)L}{D}\right] \right\} \right). \tag{A21}$$

We are then left with integrals over ϵ' and r',

$$\left(\frac{\partial n_{e^+}}{\partial \epsilon}\right) = \frac{2R \langle \sigma \upsilon \rangle \tau_E}{\pi^{1/2}(m_\chi \epsilon)^2} \int_{M_{\min}}^{M_{\max}} f^2_{\mathrm{NFW}}(c, M) \frac{\mathrm{d}n_D(M)}{\mathrm{d}\log M} \mathrm{d}\log M$$
$$\times \int_\epsilon^\infty \mathrm{d}\epsilon' \left[D(v, v') \right]^{-3} \frac{\mathrm{d}\phi}{\mathrm{d}\epsilon'} H(L, D(v, v'))$$
$$\times \int_0^\infty \mathrm{d}r' \frac{0.86}{(1 + (r'/R))^2}$$
$$\times \exp\left(-\frac{\mathrm{R}_\odot^2 + r'^2}{[D\,(v, v')]^2} \right)$$
$$\times I_0 \left(\frac{2\,\mathrm{R}_\odot r'}{[D\,(v, v')]^2} \right), \tag{A22}$$

which we evaluate numerically.

Finally, using equation (A22), we obtain the local positron flux resulting from neutralino annihilations to be

$$\left(\frac{\mathrm{d}\Phi_{e^+}}{\mathrm{d}\epsilon}\right)_{\mathrm{local}} = \frac{\beta c}{4\pi} \left(\frac{\mathrm{d}n_{e^+}}{\mathrm{d}\epsilon}\right)_{\mathrm{local}}, \tag{A23}$$

where βc is the speed of a positron of energy ϵ.

APPENDIX B: RELATION BETWEEN c_{vir} AND c_{nfw}

Here, we derive an equation relating the virial concentration c_{vir}, defined by equation (9), and the concentration c_{nfw}, defined by equation (10).

The virial mass M_{vir} is defined so that a clump of radius r_{vir} encloses a mean density $\Delta_{\mathrm{vir}}\,\rho_{\mathrm{c}}$. Therefore,

$$M_{\mathrm{vir}} = \frac{4\pi}{3} \Delta_{\mathrm{vir}} \rho_{\mathrm{c}} r_{\mathrm{vir}}^3. \tag{B1}$$

For clumps with the NFW density profile

$$\rho_{\rm nfw} = \frac{\rho_0}{(r/r_{\rm s})[1+(r/r_{\rm s})]^2}, \tag{B2}$$

we obtain the following independent expression for the virial mass:

$$\begin{aligned} M_{\rm vir} &= \int_0^{r_{\rm vir}} 4\pi\rho_{\rm nfw}(r)\,{\rm d}r \\ &= 4\pi\rho_0 r_{\rm s}^3\left[\ln(1+c_{\rm vir}) - \frac{c_{\rm vir}}{1+c_{\rm vir}}\right]. \end{aligned} \tag{B3}$$

Invoking the constraint $\rho_{\rm nfw} = 200\rho_{\rm c}$ at $r = r_{200}$, we obtain the following expression for ρ_0:

$$\rho_0 = 200\,\rho_{\rm c}\,c_{\rm nfw}(1+c_{\rm nfw})^2. \tag{B4}$$

Therefore, substituting equation (B4) into equation (B3) and equating it to equation (B1), we obtain the required relation

$$\frac{c_{\rm vir}^3}{\{\ln(1+c_{\rm vir}) - [c_{\rm vir}/(1+c_{\rm vir})]\}} = \frac{600\,c_{\rm nfw}(1+c_{\rm nfw})^3}{\Delta_{\rm vir}}, \tag{B5}$$

which must be solved numerically.

This paper has been typeset from a TEX/LATEX file prepared by the author.